ADVANCED ENGINEERING MATERIALS

DOI: 10.1002/adem.201400122

Sol–Gel Derived Fe-Rich Matrix Composites Having Precipitated WC**

By *Esteban A. Álvarez, José García,* Edgardo R. Benavídez* and *Carlos J. R. González Oliver**

The very important W−C−Co system forms the basis of the hard metal industry. Hard metals are industrially produced by powder metallurgy techniques, involving mixing, pressing, and sintering of powder mixtures. Very extensive experimental studies of the W−C−Co system have been carried out concerning – among others – synthesis, tungsten carbide (WC) grain formation and grain growth, densification, oxidation and corrosion resistance, and mechanical and thermo-physical properties.[1–9] In some applications ultrafine or fine-grained WC is needed. However, one of the main challenges is to produce carbide raw materials with ultrafine particle size and to retain the fine carbide structure after the sintering process. Chemical techniques have been developed to produce either nanoscale WC (particle size of WC < 100 nm) or nanoscale WC−Co mixtures, which are suitable for further densification into so-called nanoscale WC−Co hard metals (particle size WC ≈ 200 nm) with improved mechanical properties.[10,11] For instance nanoscale or ultrafine WC precipitated in a Co matrix has been produced by decomposition of a mixture containing ammonium paratungstate (APT), polyacrylic acid polymer (PAN), and Co-nitrate at low temperatures (750–900 °C) under a flow of H_2−Ar.[10]

Fe-alloys and others based on Ni/Co, Ni/Cr, Ni/Cr/Mn have been proposed to replace partially or totally the Co binder because of very significant cost-reduction and acceptable mechanical properties in certain application areas. Co-free binder systems have gained again in interest in the last years due to new health legislations, which restrings the use of cobalt.[12–15]

So far there are few investigations concerning the production of WC−Fe materials through chemical routes. In a previous work, we have shown that for the W−C−Fe system it was possible to formulate precursors (using W- and Fe-alkoxides), which are essentially amorphous after drying. After subsequent heating in a H_2−Ar atmosphere up to about 965 °C, WC and Fe_3W_3C phases precipitate in the Fe matrix to form dense WC−Fe composites.[16]

In the present work, the W−C−Fe system is further investigated starting from similar new sol–gel masses having now adjusted C-additions using colloidal carbon. The compositions were chosen with rather high levels of Fe binder (in the range 15–50 vol%) to make sure that WC precipitates in important quantities in order to facilitate the study of the process of nucleation/growth of WC and other phases in the Fe-rich matrix. The sol–gel masses were heat treated with different time–temperature cycles to study phase formation and phase evolution in the W−C−Fe system. The final microstructure was characterized focusing on formation, distribution, composition, and particle size of precipitated phases.

1. Experimental

The sol–gel W−C−Fe mixtures (Table 1) were prepared as described in ref.[16] For 1 g of total W + Fe metals (based on W $(OC_2O_5)_5$ and modified Fe-propoxide), 4 g of copolymer P123 (poly(ethylene glycol)-block-poly(propylene glycol)-block-poly(ethylene glycol) [435465 Aldrich, MW5800]) and colloidal carbon were added. These precursors were blended for periods of 16–24 h. After blending, the mixtures were dried at 80 °C. The dried powders were grinded manually (agate mortar) to produce the final powder and pellets were pressed for sintering. Sixty-five milligrams of C (colloidal graphite)

[*] *Dr. J. García*[+]
AB Sandvik Coromant R&D, SE-12680, Stockholm, Sweden
E-mail: jose.garcia@sandvik.com
Dr. C. J. R. González Oliver
CONICET, Avenida Rivadavia 1917, RA-1033, Buenos Aires, Argentine
E-mail: gon@cab.cnea.gov.ar
E. A. Álvarez
Centro Atómico Bariloche – CNEA, Av. E. Bustillo 9500, RA-8400 Bariloche, Argentine
Dr. E. R. Benavídez
Departamento Metalurgia, Centro DEYTEMA, Facultad Regional San Nicolás, Universidad Tecnológica Nacional, Colón 332, B2900LWH San Nicolás, Argentine

[+] *Former address: Helmholtz Zentrum Berlin für Materialien und Energie GmbH, D-14109, Berlin, Germany*

[**] *ANPCyT (project PICT-Raices 20101759), Universidad National de Cuyo (project 06/C372) and CONICET (project PIP 1122011010053301) are acknowledged for financial support. Part of this work was carried out within the German/Argentine project "Nano-skalige Fe-Legierungen und -Komposite" (BMBF–MinCyT, ARG08/003) and the "NanoCom Network" project (FP7-IRSES Project 247524/ Saarland University). The Superconductivity and Metal Physics Groups of CAB are acknowledged for research budget for the purchase of IBT Edwards Auto 306 apparatus, parts of the Theta, Inc. dilatometer and for the use of the TEM CM200 microscope. Mr. Sanfilippo (Nuclear Materials, CAB) and Ms. P. Troyon and Mrs. C. Ayala (Materials Characterization, CAB) are thanked for technical support.*

Table 1. Chemical formulations investigated.

Code	W/Fe [weight ratio]	P123	Colloidal graphite	Al_2O_3
A1, A2, A3, A4	1.5	4 g for 1 g total metals	65 mg	–
A5	1.5	4 g for 1 g total metals	110 mg	–
B1	1.5	4 g for 1 g total metals	–	–
B2	9	4 g for 1 g total metals	–	–
C1, C2, C3	1.5	4 g for 1 g total metals	65 mg	10 mg

was added to the sample series A (A1, A2, A3, and A4). For sake of comparison, 110 mg of colloidal carbon was added to one sample of series A (composition A5). To investigate the influence of Al_2O_3 additions on the synthesis (densification and grain growth), 10 mg of alumina was added to sample series C (C1, C2, and C3). The alumina was nanometric aeroxide (size of the alumina particles is ca. 6 nm, aluminiumoxid C) from the late Degussa-Hüls, Germany. These additions correspond to approximately 12% C (all compositions in this study are given in wt%) and 2% alumina to the total WC nominally formed. In particular, the effect on phase formation due to the presence of stable Al_2O_3 and the possibility of adding another nanosized hard phase in the sintered WC−Fe microstructure (oxide dispersion strengthening effect) was investigated. The equivalent 1 g total metal comes from a fixed ratio of W and Fe precursors. The total C content is a result of the alkyl precursors (W, Fe, C, and O) and the additions of colloidal carbon. The total carbon content in these precursors was not measured. In general, the control of the final carbon content of WC–metal mixtures is extremely difficult, since the carbon window to avoid the formation of subcarbides (C-poor composition) or free graphite (C-rich compositions) is very narrow (for a typical WC−Fe system varies between 5.51 and 5.59% carbon; i.e., the carbon window is 0.08%). In R&D and industrial production using conventional powder metallurgy, the carbon is adjusted by trial and error. In general "extra" carbon is added to the mixtures to compensate the carbon lose during sintering due to the reduction of oxides during the vacuum sintering step. In our work, the carbon content was also adjusted by simple trial and error. It is possible to adjust how much colloidal C (or addition of specific polymers) must be added to have the correct phase formed depending on the sintering cycle. The B sample series (B1 and B2) are Fe–W mixtures without additional colloidal carbon.

In order to produce pellets out of the fine powder, an agglutinant was used. Two percent PVB (MW 150,000, polyvinyl butyral; Polyscience, Inc., USA) was added to the previous powder mixtures. Pellets of ca. 100 mg were pressed uniaxially in a steel mould at approximately 240 MPa for 2 min. Pellets were heat treated in a laboratory furnace (Table 2). The sealing parts of the furnace were carefully adjusted to achieve good vacuum conditions at high temperatures. The heat treatment cycles (HT) included an initial heating step (3–5 °C min^{-1} heating rate) under a flow of 10% H_2−Ar up to about 600–800 °C. A second heating step at a similar rate up to generally 1250–1360 °C under maximum vacuum (0.03–0.07 mbar) was carried out. The holding time at the maximum temperature was 2 h. All samples were cooled at furnace rate till room temperature (RT). In the heat treatment HT1 the specimens were kept 90 min at 400–645 °C under vacuum before the second heating step up to 645–1360 °C was started (due to an adjustment of the sintering furnace). The oxygen content in the sintering furnace during the process was not measured. However, a WC−Co specimen (produced with 0.3 μm WC from H.C. Starck and 20% Co powder from Merck) was sintered simultaneously to check the formation of subcarbides or oxides due to insufficient vacuum conditions. No evidence of presence of oxygen in this specimen was found such as the formation of η-type phases (which may indicate some decarburization of WC) or oxygen containing phases like CoO or $WCoO_4$.

Table 2. Heat treatment schedules.

Codes	Initial heating step (10% H_2−Ar flow)	Final heat treatment step (vacuum of 0.03–0.07 mbar)	Time at max. temperature [h]
HT1[a]	3 °C min^{-1} RT-645 °C	3 °C min^{-1} 645–1360 °C	2
HT2	3 °C min^{-1} RT-760 °C	3 °C min^{-1} 760–1360 °C	2
HT3	3 °C min^{-1} RT-600 °C	3 °C min^{-1} 600–1350 °C	2
HT4	3 °C min^{-1} RT-800 °C	3 °C min^{-1} 800–1350 °C	2
HT5	3 °C min^{-1} RT-800 °C	5 °C min^{-1} 800–1250 °C	2
HT6	5 °C min^{-1} RT-1090 °C	–	1
HT7	5 °C min^{-1} RT-965 °C	–	1

[a] Specimens were kept at 400–645 °C under vacuum for 90 min before starting the second heating step.

Phase formation was investigated by X-ray diffraction (XRD) using a Philips PW1700 diffractometer (Cu wavelength 0.154054 nm). Sintered pellets were grinded on the surface to remove any possible contamination before XRD analysis. The specimens were aligned parallel to the camera reference planar surface in the XRD system. Silicon particles were

DOI: 10.1002/adem.201400122

ADVANCED ENGINEERING MATERIALS

spread onto representative samples to calibrate 2θ in the patterns. The particles were deposited onto the surface of the specimens by dropping one drop of diluted Si/iC_3H_7OH ultrasonically dispersed mixture. It is not consider that this may affect the error of the 2θ by divergent irradiation. The diffraction patterns were analyzed by the commercial program X'Pert HighScore. Scanning electron microscopy (SEM) analyses were carried out with a Philips SEM 515 and a SEM-FEI Nano-Nova equipped with electron dispersive spectroscopy (EDS) and transmission electron microscopy (TEM) with a Philips CM200. TEM thin foils preparation was carried out with an IBT Edwards Auto 306 apparatus. Ar^+ ions were accelerated at 5 kV and the beam acted at an angle of 12°, relative to the rotating surface of the sample, for about 16 h. Finally, a cleaning-etching at 2 kV for 30 min was applied. This procedure was carried out in order to avoid damage of the thin foil. Some TEM samples were prepared with a focused ion beam (FIB) at Saarland University using a FIB/SEM dual beam Workstation Helios Nanolab 600 (FEI). Cross-sections of samples were prepared for metallographic studies (light and SEM). Samples were cut with a diamond saw, embedded in resin, and polished manually using diamond impregnated polymer films (South Bay Technology, USA). The final diamond size was 1 μm (10 min polishing). Instantaneous height of the specimens during densification was measured with a Theta Dilatromics II (USA) dilatometer.

2. Results

2.1. Phase Formation within the Resulting Fe-Rich Matrix

Results of sol–gel specimens having extra carbon added as colloidal C, with and without the addition of colloidal alumina, produced with the two steps heat treatment are presented. XRD patterns of various precursors having nominally weight ratios of W/Fe = 1.5 containing different amounts of extra carbon added on purpose and after various heating schedules up to 1250–1360 °C are shown in Figure 1. The diffraction peaks for A1-HT1 (without Al_2O_3) and C1-HT1 (containing colloidal Al_2O_3) heat treated simultaneously according to HT1 (1360 °C) clearly show that WC has formed in both cases. Fe may be present as indicated by the weak peaks at 44.67°. Free carbon is present in C1-HT1 and C2-HT2, as indicated by the peaks at around 26° [C, JCPDS 001-0646]. Both samples C1-HT1 and C2-HT2 were quite porous, as it will be analyzed in Section 2.2 for companion compositions, and no effect on precipitated phases was observed by changing the heat treatment temperatures, since the XRD patterns were nearly identical. The added volume fraction of alumina particles is rather low and consequently the detection of its corresponding XRD crystalline diffraction peaks is limited.

In relation to the presence of free Fe in these specimens, it should be noted that for the composition A5-HT5 (110 mg colloidal C/final temperature of 1250 °C/2 h) well-defined Fe and C peaks as well as the precipitated WC reflections were measured. After the densification at the highest temperature of about 1360 °C, the specimen series C (containing nanoscale alumina grains) exhibited clearly lower densification and presented higher porosity in the microstructure compared to the A series compositions having no Al_2O_3 additions. It could be suggested that for sol–gel systems, the alumina grains also arrest densification, as observed in conventional WC–metal systems produced by powder metallurgy processes. However, in the sol–gel mass containing the alumina particles, both the Fe-rich matrix and WC nuclei precipitate gradually during the heating step, which is a densification situation that contrasts strongly with that observed for powder mixtures of binder and WC.

The diffraction patterns of specimens A2-HT3, A3-HT4, and C3-HT3 (all having Si particles spread onto the surface for 2θ°calibration purposes) are shown in Figure 2. It is noted that the WC-peak positions correspond almost exactly with the WC-theoretical values (JCPDS 025-1047; hexagonal: a = 0.29062 nm, c = 0.28378 nm). Very few Fe peaks were detected. In samples without added alumina (A2 and A3), the M_6C

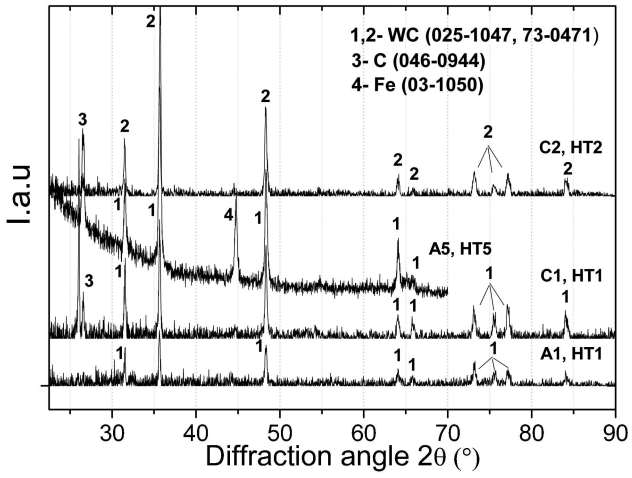

Fig. 1. XRD of sol–gel materials A1-HT1, A5-HT5, C1-HT1, and C2-HT2.

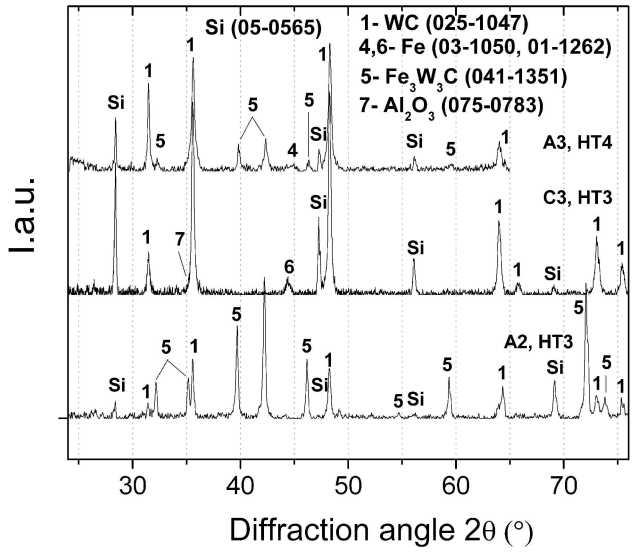

Fig. 2. XRD patterns of sol–gel materials with (C3) and without (A2, A3) Al_2O_3 addition.

DOI: 10.1002/adem.201400122

phase Fe_3W_3C (JCPDS 041-1351; cubic, $a = 1.11094$ nm) was detected. The alumina addition may influence the formation of the subcarbide phases; for the present samples addition of alumina avoids the formation of subcarbide phases like M_6C (see Figure 1 and 2). It can be observed that the amount of M_6C subcarbides formed is drastically reduced by increasing the final temperature of the initial heat treatment – compare 600 °C (A2-HT3) to 800 °C (A3-HT4). Sample A1-HT1 (Figure 1) seems not to follow this trend; however, the cycle HT1 differs considerably from HT3 and HT4 since a holding time of 90 min (400–645 °C/vacuum) was introduced in HT1. Specimen C3-HT3 shows a very small Fe peak, WC peaks and no subcarbide phases such as M_6C (W_3Fe_3C). A XRD peak corresponding to the Fe reflection was observed. The reasons for the low intensity of the Fe reflections may be attributed to the fact that the XRD was collected from the clean surface of the sample and not from comminuted specimens (powder diffraction) due to the fact that specimens were very hard and it was not possible to grind them into fine powder. Another explanation is that only the outer surface part of the sample could be examined with the X-rays (due to the high absorption of WC) and that in those areas the Fe levels could be lower than expected due to some volatility or segregation of Fe. The permeation and evaporation is a general issue when sintering in vacuum in the presence of liquid phase. This phenomenon could produce also what is called "binder-capping" in hard metals, i.e., the formation of a metal layer on top of the sintered piece, which eventually can be eliminated by evaporation at higher vacuum sintering conditions. The formation of free Fe or Fe-containing phases depends on the final sintering temperature. For example, in sample A5-HT5 (final temperature 1250 °C), the XRD peak of free Fe was of considerable intensity. On the contrary for all specimens heated at 1360 °C (final temperature), very small signals of Fe were detected by XRD (see diffractograms A2-HT3 and A3-HT4) but important quantities of Fe containing subcarbide phases.

Sol–gel masses without the addition of colloidal graphite (B1 and B2) heat treated up to 965 °C under a 10% H_2-Ar flow for 1 h (HT7) were examined by XRD (Figure 3). In sample B1-HT7, it is noted that the WC phase did not form but the phases $M_{12}C$ (Fe_6W_6C) and free Fe. This may be a consequence of a C-deficient material, since no extra colloidal graphite was added. On the contrary for specimen B2 – which has an initial W/Fe ratio of 9 – no free Fe is detected. Some reflections corresponding to WC and M_6C (Fe_3W_3C) were detected, but also some W_2C and some W metal reflections. The presence of sub-carbides suggests that the system is C-deficient. The ratio of subcarbides M_6C and $M_{12}C$ differs significantly between B1-HT7 and B2-HT7. This is an indication that sample B2 has more active (excess) carbon than B1. However, as discussed above, the measurement of carbon is difficult due to the small amount of these samples (ca. 100 mg). Furthermore, the carbon measurement in the various precipitated phases, like the polycrystalline WC can be underestimated due to the dead time of the detector, mainly affecting C estimations since it can

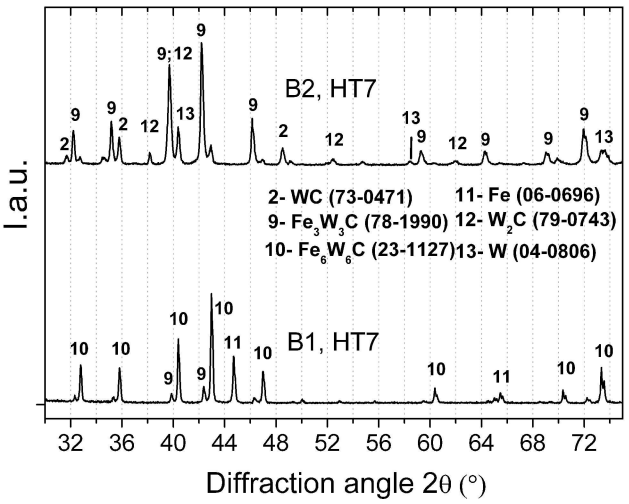

Fig. 3. XRD patterns of sol–gel materials without addition of colloidal graphite (B1 and B2) after heat treatment under a flow of 10% H_2-Ar up to 965 °C (1 h).

evaporate as multiple ions.[17] Summarizing and as quoted in our previous study in ref.[16] samples B1 and B2 heat treated with HT7 present roughly the following percentages of precipitated phases: 53.4% Fe_6W_6C, 12.2% Fe_3W_3C, 34.4% Fe (B1); and 55.4% Fe_3W_3C, 27.6% W_2C, 3.7% WC, and 13.3% W (B2).

Finally, the specimen A4-HT6 densified in the dilatometer is considered in this section (Figure 4). In Figure 4a, the XRD pattern of the final specimen after 1 h at 1090 °C under a flux of 10 %H_2-Ar is shown. The phases WC, W and C are observed. However, the main phases present are W and C showing that the specimen underwent important decarburization due to the interaction with the 10 %H_2-Ar at high temperatures. The presence of $M_{12}C$ is not excluded since its main reflections (JCPDS 23-1127) are close to 40.416°, which is the most intense peak for W (JCPDS 08-0406). Only a very small peak for pure Fe is observed. In Figure 4b, the curve for the absolute densification ($\Delta l/\mathrm{lo}$) versus T (°C) of the pellet is shown. $\Delta l/\mathrm{lo}$ is given by the following Equation (1):

$$\frac{\Delta l}{\mathrm{lo}} = \frac{(l(T,t) - \mathrm{lo})}{\mathrm{lo}} \quad (1)$$

Important features in $\Delta l/\mathrm{lo}$ are measured for $T > T1 = 815$ °C. Before going into detail, it should be noted there is some contraction at around 530 °C and that so far it is not known the nature of it. From $T > T1$, the pellet expands stopping at $T2$. At $T3$, it shows a clear contraction or densification and at $T4$, the contraction stops/slows down very markedly. Finally at ca. 975 °C, it speeds up its densification again. This is an indication of a remarkable solid state sintering process and it is further discussed in Section 3.3.

2.2. Microstructure Investigations

SEM images of samples A1-HT1 and A3-HT4 are shown in Figure 5. The main phase in both samples is WC (light gray) as

ADVANCED ENGINEERING MATERIALS 2014,
DOI: 10.1002/adem.201400122

ADVANCED ENGINEERING MATERIALS

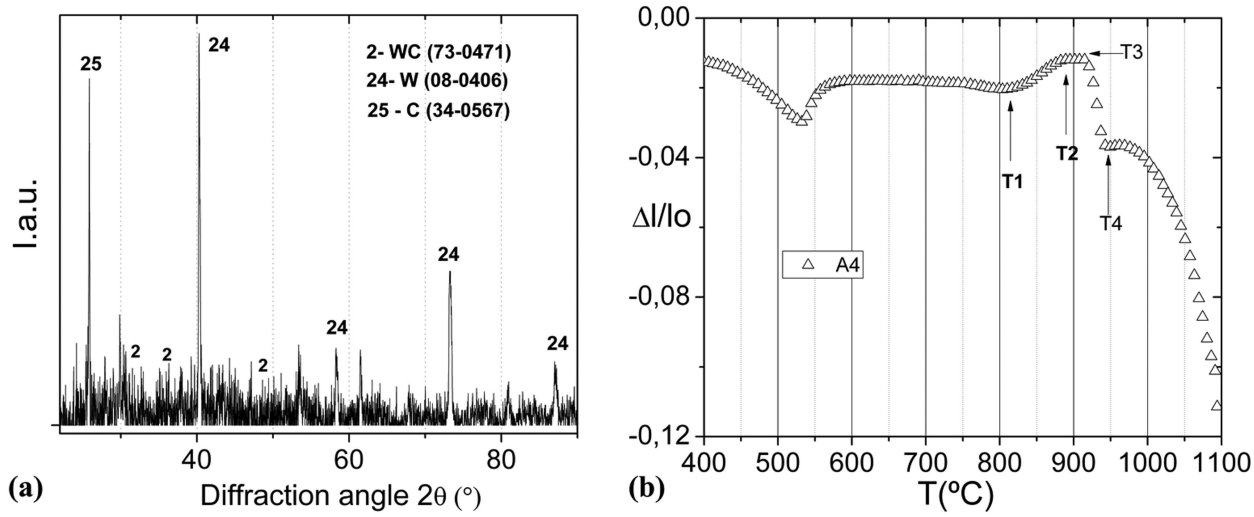

Fig. 4. (a) XRD of specimen A4-HT6 (1090 °C, 10%H_2–Ar, dilatometer). (b) Densification of A4-HT6.

confirmed by SEM–EDS point analysis. It can be observed that sample A3-HT4 presents a higher volume fraction of smaller WC grains (compare Figures 5a and b). The average WC particle size (linear intercept method) in sample A1-HT1 is ca. $4.5 \pm 0.5\,\mu m$ whereas in sample A3-HT4 is $2.5 \pm 0.5\,\mu m$. The second phase (dark gray/black) in A1-HT1 corresponds to the Fe binder phase, which presents W (1.5%) and C (10%) dissolved in it. The binder phase in sample A3-HT4 is a mixture of Fe and Fe_3W_3C as confirmed by XRD analysis. As already mentioned, the microstructures of the sintered samples are in general not homogeneous. As example, microstructure common characteristics of samples A5-HT5 and A1-HT1 are shown in Figure 6. Sample A5-HT5 had excess carbon added in colloidal form. After sintering, the phases WC, Fe, and C were identified by XRD (see Figure 1). A junction of three grains (large dark grains) of WC and a small grain of matrix can be observed in the TEM bright field image in Figure 6a. Several defects like dislocations can be seen in the light-gray WC grain on the right hand side. The top black-like WC grain is oriented in a $[1\bar{1}02]$ zone axis orientation and has an average size of 2000 nm. Figure 6b shows a different area of sample A5-HT5 where thick black layers of carbon (I) surround some matrix material. This carbon remains unreacted during the heat treatment process. Also a large WC grain on the bottom part is observed (II). SEM–EDS point-analysis of the WC grain resulted in an elemental composition of 95.09% W, 0.97% C, and 3.94% Fe. The matrix composition measured was: 82.76% Fe, 15.77% W, and 1.47% C. In the region of the thick carbon band, the composition obtained was: 83.23% C and 16.77% Fe. It is proposed that the grain of WC could be doped with iron, and that considerable contents of W are dissolved in the Fe matrix. The excess of carbon formed clearly a separate phase in the A5-HT5 sample. In Figure 6c, the TEM micrograph of sample A1-HT1 shows five or six large WC grains having dislocations and eventually some precipitates inside these dislocations (labeled as I). Areas of spongy type Fe-pockets (light gray) are also observed (labeled as II). The remaining bright areas are pores and Fe-pockets where the Fe was probably etched by the Ar^+ ion beam during the milling operation. Between the top black WC

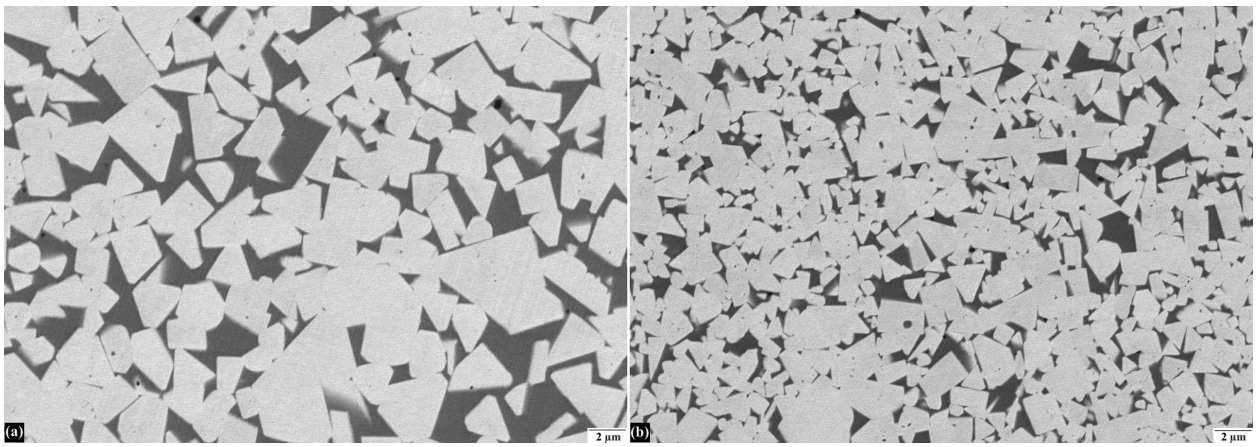

Fig. 5. SEM micrographs of sol–gel derived WC–Fe composites (a) A1-HT1 and (b) A3-HT4.

DOI: 10.1002/adem.201400122

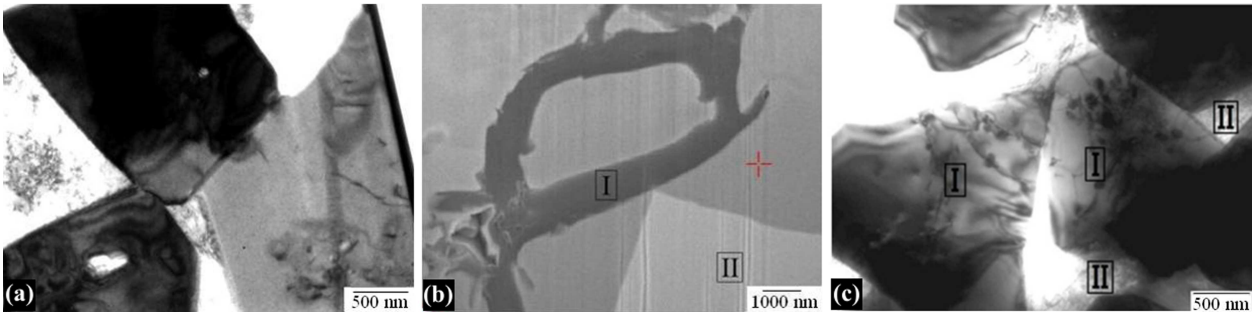

Fig. 6. (a) Sample A5-HT5, TEM micrograph 1250 °C. The thin foil for TEM was prepared by polishing with Ga ions (FIB). (b) A5-HT5, image obtained by SEM. EDS analysis is 1.47% C, 82.76% Fe, 15.77% W in label (+); 83.23% C, 16.77% Fe in label [I], and 95.09% W, 3.94% Fe, 0.97% C in label [II]. (c) TEM of A1-HT1, [I] WC grains, [III] Fe binder. TEM thin foil thinned down by Ar^+ ion beam milling.

grain (oriented in a zone axis direction) and the WC grain (toward the middle of the image) a well-defined thin interface has formed. A thicker interface or thin band of ca. 30 nm in thickness separating the Fe-matrix and WC phases is observed. The EDS analysis in SEM mode showed traces of Fe inside the WC and some W inside the Fe-pockets, similar to the ones reported above for material A5-HT5 presented in Figure 6b. SEM images of sample C3-HT3 – with alumina additions – showed low density due to reduced densification (Figure 7). High porosity and relatively small WC grain size can be observed. SEM–EDS analysis measured a composition of 82% W, 2% Fe, and 15% C in position A, 15% Al, 15% C, 61% Fe, and 8% W in position B, and 11% C, 9% Al, 47% Fe, and 32% W in position C. Additionally another sample (C2-HT2– also containing alumina) was examined by SEM showing the formation of WC grains (label D, 85% W and 15% C) in a Fe-rich matrix (label E, 76.5% Fe, 11.4% Al, 7.4% C, and 4% W) with also the presence of some isolated Al_2O_3 particles surrounding WC grains (circle F). The slight differences on the compositions can be explained by the fact that the samples are from different batches and heat treatments and also the analysis were carried out with different set ups and SEM devices (Philips/Nova nano-FEI).

3. Discussion

The discussion focuses on the phase formation, conversion paths of the sol–gel mixture into WC−Fe composites and densification of the sol–gel masses. Results are compared to established theories of sintered WC–metal systems produced by conventional powder metallurgy.

In the WC−Co and WC−Fe systems produced by conventional sintering, the liquid phase forms at the eutectic temperatures of ca. 1300 and 1140 °C, respectively. Co dissolves approximately 10–22% WC whereas Fe only dissolves 7.5% WC at 1143 °C.[6,12,18–21] The densification of WC−Co hard metals (with binder volumes ranging between 5 and 30 vol% Co) begins under solid state diffusion conditions below the eutectic temperatures. This stage covers roughly 20% densification for conventional micro-sized WC or to 80% extent for nanosized WC.[4,22] Extensive WC grain growth takes place during this stage,[22] which is the main difficulty to maintain the nanoscale/fine grain microstructure. The final sintering stage is an isothermal treatment at ca. 1400 °C. This densification stage is under the action of a liquid phase rich in Co whereby the WC must dissolve in the liquid. Therefore, the final densification extent is controlled by diffusion of W and C

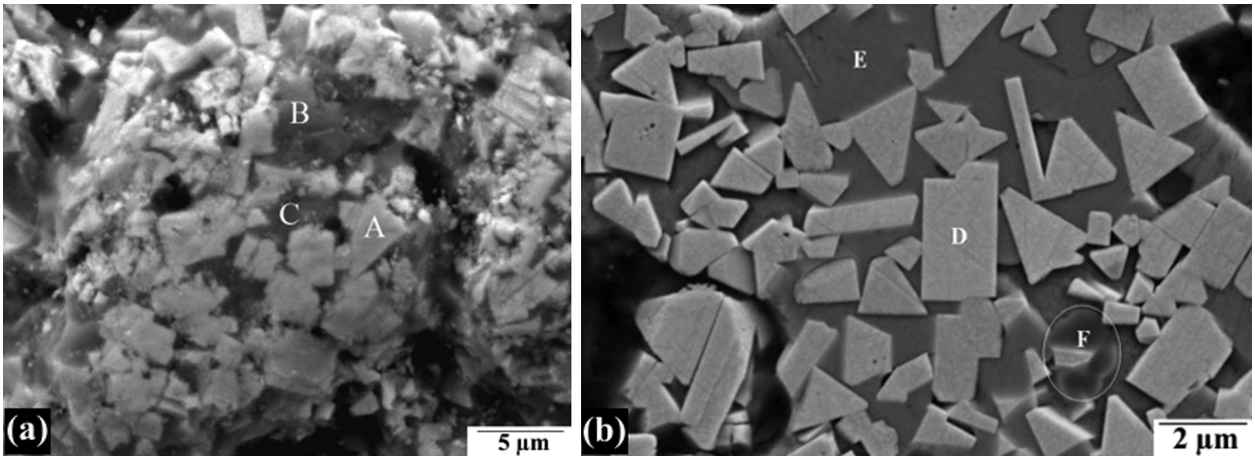

Fig. 7. SEM images of (a) fracture surface – roughly polished – of sample C3-HT3. (b) polished sample C2-HT2. Black regions are porosity.

DOI: 10.1002/adem.201400122

ADVANCED ENGINEERING MATERIALS

in Co and the precipitation/re-precipitation of WC causing the particle center-to-center approach increasing density and further grain growth. Another important effect in the microstructure of WC−Co is faceting of the WC-grains and this depends on the liquid content and temperature/atmosphere/period of time of sintering.[23] Owing to the tendency toward grain growth, WC−Co compositions are usually modified by addition of for instance VC or Cr_2C_3 (0.2–0.5%), which act as grain growth inhibitors but also increase the tendency to brittleness of the composites.[22]

3.1. Conversion Paths from Amorphous Sol–Gel Mixtures into Crystalline WC−Fe Composites

Prior to address possible paths for the conversion of the W−C−Fe−O sol–gel amorphous masses into crystalline WC−Fe composites, it could be relevant to quote chemical developments in the clearly more studied WC−Co system. These investigations describe the use of inorganic metal compounds as sources of W and Co. Ammonium tungstate or tungstic acid, polyacrylonitrile (PAN), and Co nitrate has been used as sources of W, C, and Co.[10,11,24] Gao and Kear[24] heated WO_3 or ammonium tungstate up to 700 °C under a flow of H_2/CO (2:1 ratio). From thermogravimetric measurements data, it was detected that reduction of WO_3 begins at around 500 °C. Zhu and Manthiram[10] observed that whether the prior air-decomposition of PAN (275–470 °C) neither a subsequent firing (4–10 h at 950 °C) influenced strongly the amount of undesirable subcarbide phases (W_2C, Co_6W_6C, and Co_2W_4C) as well as the formation of pure W metal. The catalytic effect of Co on the formation of WC was confirmed. Also mixtures of PAN, tungstic acid and $Co(NO_3)_2 \cdot 6H_2O$ were dried at 300 °C in air and heated for 1 h at 800, 900, and 1000 °C under a flow of 10% H_2−Ar.[11] WC embedded in a Co matrix was obtained, however contaminated with W_2C, W, and WO_2. The proposed sequence for WO_3 reduction was: $WO_3 \rightarrow W_{18}O_{49} \rightarrow WO_2 \rightarrow W \rightarrow W_2C \rightarrow WC$. A similar path was described by Liang et al.[25] by synthesizing the W_2C phase for catalytic purposes. Hudson et al.[26] measured that the reduction of WO_3 with hydrogen (at reduced pressures) promotes the formation of W^{5+} ions in a first step and W^{4+} ions in a second step (which form clusters of W^{4+} due to metal–metal bonding). Haber et al.[27] heated mixtures of sodium tungstate and ammonium poly(acrylic acid) in Ar at 900 °C for 2 h. Upon cooling WO_x, WC, and traces of Na_xWO_3 were obtained.

A possible conversion path in our system is that WC nucleates continuously in a Fe-rich solid matrix, which has also been formed continuously during the removal of oxygen from the system (due to the reaction with hydrogen during the first heat treatment). If a high homogeneous distribution of W and Fe can be assumed (owing to the homogeneous bonding/mixing of metal alkoxides) and probably further homogeneous hydrolysis/condensation reactions between the metal alkoxides take place (similar to the types involved in alkoxide gel-formation under acid conditions, which lead to percolated three dimensional network of M(metal)−O−C bonds),[28–31] then a kind of supersaturated W−C−Fe−O amorphous matrix should have formed. Under the correct C-activity, the oxygen reduction (given by the action of hydrogen) should activate the W-carburization stage. By this process, WC embryos/nuclei should form within such evolving matrix. It could be expected that some defects are formed/trapped within the growing WC grain. Indeed in Figure 6a and c, dislocations and perhaps stacking faults are detected within the large WC crystals; however, these defects have not been studied in detail yet. TEM studies also confirmed the formation of WC–WC interfaces in the W−C−Fe system, which is also a characteristic in the W−C−Co system.[6,23,32] TEM analysis of both samples A5-HT5 and A1-HT1 show that WC grains are single crystal. Some nanosized pores are observed within the WC grains, which may be a consequence of the nucleation and growth process out of the iron rich matrix. In some WC grains, a reaction layer of about 30 nm in thickness formed between the WC and Fe phase. The growth of the WC grains is of facet/acicular type, which are typical of WC growing in the presence of large quantities of binder phase.[23]

As reported in several works in the WC−Co system,[1,22] nanoscale WC grains grow extensively even during the solid state sintering step, due to the fact that the main driving force for sintering is the reduction of free surfaces. In the present W−C−Fe−O precursors – after reduction of oxygen at low temperatures in the range 500–800 °C – the nanoscale WC-grains grow rapidly (by solid state diffusion) and the nanoscale structure may be quickly lost unless grain growth is stopped. Furthermore for $T > 1150$ °C, the WC grains are in contact with the Fe-rich liquid phase and the WC grains will grow further, facet and coarsen rapidly.[22,23,32] It should also be noted that Al_2O_3-additions to the WC−Fe system causes a strong densification arrest as judged by the porous C-specimens (C1-HT1, C2-HT2, and C3-HT3). It was also observed that additions of alumina avoid the formation of subcarbide phases like M_6C. Microstructure features by Al_2O_3-additions (see Figure 7) are currently investigated by TEM with the aim of determining whether the colloidal alumina was dispersed homogeneously in the as-formed spongy Fe-rich matrix through the reduction of the W−C−Fe−O precursor.

3.2. Phase Formation by Different Heat Treatments

In this study, we aim at showing that starting from *amorphous* sol–gel powders it is possible to produce *in situ precipitation* of WC within a Fe-rich matrix; offering the possibility of producing fine grain WC embedded in a Fe-matrix due to the nucleation and growth processes acting in the amorphous matrix. From the above reported data for the sol–gel derived WC−Fe materials, it has been demonstrated that by sintering in the range 1250–1360 °C (10% H_2–Ar + vacuum), it is possible to form a composite consisting in a Fe-rich metal matrix reinforced with WC or subcarbides (see Figure 1). The sol–gel W−C−Fe−O moieties must be first reduced; the WC and Fe phases precipitated and finally the

DOI: 10.1002/adem.201400122

system must be densified. Therefore, it is necessary to use both the H_2-Ar mixture and subsequent vacuum to form dense WC–Fe specimens. Furthermore, the H_2-Ar gas mixture cannot be used throughout the whole sintering schedule as the W-intermediate oxides or carbide moieties will be irreversibly reduced/decarburized to mainly pure W, Fe, and W–Fe phases.

Significant to this research work are the XRD results in Figure 2 where the 2θ (°) calibrated XRD-patterns showed no shifts in the elementary *a*- and *c*-values of the hexagonal unit cell of WC. This may mean that WC is not doped with Fe.

The present vacuum densification (up to 1250–1360 °C) after the initial heat treatment (up to mainly 600–800 °C under flowing H_2-Ar gas to remove oxygen from the system) has proven to be very useful to consolidate the sol–gel mixtures. The nearly dense samples A1-HT1 and A3-HT4 (Figure 5) confirm the suitability of our approach to produce WC–Fe composites using the described sol–gel formulations and densification techniques.

It is worth noting that for specimen A5-HT5 having excess carbon (Figure 6) the phases formed in the W–C–Fe system were analyzed by SEM–EDS. Three phases were observed: WC apparently doped with traces of Fe (2–4% Fe); binder with 84% Fe and 16% W, and carbon layers or flakes with a composition 83% C–17% Fe. However, it should be noted that these results correspond to a clearly *heterogeneous* specimen (A5-HT5), which sintered to quite perfect areas, showing defined WC-grains, Fe-rich matrix, and very small areas rich in C, as shown in Figure 6a. In some cases the unreacted carbon is present in the form of very thick layers of carbon (containing some Fe) as shown in Figure 6b.

This specimen is of significant relevance because after the rather low sintering temperature of 1250 °C, the aimed Fe-rich matrix and full precipitation of WC is already obtained.

A remarkable influence of the final sintering temperature and excess carbon on porosity was observed. Lower and more appropriate C-contents in the A-specimens heat treated at 1360 °C allowed for denser microstructures compared to the heat treatment at 1250 °C.

In the W–C–Fe compositions in this work (Table 1), the binder level can be nominally as high as 50 vol%. The final temperatures (Table 2) might be higher than needed (considering the eutectic point of the system WC–Fe), which may explain the extended grain growth observed. Therefore, if a nano or fine grain structure is desired, a further adjustment of the sintering temperatures of the process described in this study is necessary to tailor the final particle size of the WC phase. Another possibility is to use a rapid consolidation technique such as spark plasma sintering where the time at the highest sintering temperature is considerably reduced allowing the production of finer microstructures.[32]

3.3. Densification Features

Our previous study on W–C–Fe–O gel masses having additions of colloidal C in the temperature range 530 °C $< T \leq$ 815 °C has shown that the system is probably formed by some free Fe and mainly $WFeO_4$, hence the oxygen comes from trapped water in the sol–gel mass and from the alkoxy moities of the W and Fe alkoxides.[16] These phases were detected by XRD on specimens heated up to about 1000 °C under vacuum.[16] By DTA measurements (under a flux of pure Ar), endothermic/exothermic peaks were detected at 400 and 700 °C, which are probably associated to formation of the previously mentioned Fe and $WFeO_4$ phases. The runs under H_2 should still allow the formation of Fe but also subcarbides (or even WC) may form, as indicated by Chou et al.[33] In their research, amorphous films were prepared in the W–C–Fe system by electroplating on copper substrates for 1 h. The dry films were annealed in pure H_2 to avoid oxidation. The films were amorphous up to 600 °C. For higher temperatures Fe and Fe_2W precipitated and at about 800 °C, the subcarbide W_6Fe_6C phase formed. Exothermic peaks at 377 and 620 °C were obtained by differential thermal analysis (DTA). Furthermore, it was suggested that at temperatures lower than 300 °C the films were amorphous and that for the temperature range 400–600 °C, there is a co-existence of amorphous and nano-crystalline Fe.

Summarizing the prior investigations and the XRD investigations of samples B1-HT7, B2-HT7 in this work (Figure 3), it has been shown that the phases WC, the subcarbide phases and Fe already form at 965 °C, indicating that phase formation in the sol–gel samples takes place during the first heat treatment cycle (reduction). A further increase of temperature (or time) at these conditions lead to strong decarburization (see example A4-HT6, Figure 4a). However, similar samples sintered with the two-step process (A1-HT1, A2-HT3, and A3-HT4) generally leads to the formation of WC, Fe, and Fe–W phases. It can be suggested that the solid state densification measured for $T \leq 950$ °C is assigned to densification of WC and Fe and/or Fe–W phases formed by the conversion of the present sol–gel masses during the reduction process; indicating that essentially solid state sintering of WC- and Fe-particles was the main operating densification mechanism.[34] The previous analysis also explain why the initial heat treatment is so effective in removing oxygen out of the system, maintaining the formed WC without any decomposition and making it feasible for further densification under vacuum in the 1250–1360 °C temperature range.

The proposed mechanism will be further investigated in a future publication focused on densification of sol–gel W–C–Fe–O masses.

4. Conclusions

WC–Fe crystalline composites were prepared from elementary amorphous sol–gel masses containing W, Fe alkoxides, and extra carbon added in solid and polymeric forms. WC precipitated in situ out of the W–C–Fe–O masses.

Densification schedules involving an initial heating step under 10% H_2-Ar up to 600–800 °C and a subsequent vacuum heating step up to 1250–1360 °C for 2 h were very useful to densify these specimens.

ADVANCED ENGINEERING MATERIALS 2014,
DOI: 10.1002/adem.201400122

ADVANCED ENGINEERING MATERIALS

TEM investigations have shown that the WC grains present a hexagonal phase facetted in morphology with some inner crystalline defects.

The Fe-rich matrix phase was nearly pure Fe for final temperatures between 965 and 1360 °C. The dense microstructures resembled closely those for standard WC–Co hard metals.

The conversion of amorphous W–C–Fe–O masses into two phases WC–Fe composites was analyzed from dilatometric expansion/contraction behavior of pellets pressed from such dried masses.

It is concluded that Fe is probably first formed and upon hydrogen treatment up to about 950 °C WC is fully precipitated together with further free Fe forming the desired Fe-rich matrix–WC reinforced composites.

Additions of Al_2O_3 to the W–C–Fe–O masses reduce densification – mainly by arresting polycrystalline WC grain growth – increase the inhomogeneity of the samples and clearly influence the formation of carbides.

Received: March 10, 2014
Final Version: May 19, 2014

[1] Z. Zak Fang, X. Wang, T. Ryu, K. S. Hwang, H. Y. Song, *Int. J. Refract. Met. Hard Mater.* **2009**, *27*, 288.
[2] F. F. P. Medeiros, S. A. De Oliveira, C. P. de Souza, A. G. P. da Silva, U. U. Gomes, J. F. de Souza, *Mater. Sci. Eng. A* **2001**, *315*, 58.
[3] R. Koc, S. K. Kodambaka, *J. Eur. Ceram. Soc.* **2000**, *20*, 1859.
[4] L. Åkesson, *Thermochim. Acta* **1979**, *29*, 327.
[5] D. Demirskyi, A. Ragulya, D. Agrawal, *Ceram. Int.* **2011**, *37*, 505.
[6] J. García, W. Lengauer, *Mikrochim. Acta* **2001**, *136*, 83.
[7] S. K. Sahay, S. B. Kumar, B. Goswami, A. K. Ray, *J. Metall. Mater. Sci.* **2007**, *49*, 143.
[8] C. Barbatti, J. García, P. Brito, A. Pyzalla, *Int. J. Refract. Met. Hard Mater.* **2009**, *27*, 768.
[9] T. Yamaguchi, M. Okada, *J. Am. Ceram. Soc.* **1977**, *60*, 289.
[10] Y. T. Zhu, A. Manthiram, *Composites: Part B* **1996**, *27*, 407.
[11] M. F. Zawrah, *Ceram. Int.* **2007**, *33*, 155.
[12] G. S. Upadhyaya, S. K. Bhaumik, *Mater. Sci. Eng. A* **1988**, *105/106*, 249.
[13] B. Wittmann, W. D. Schubert, B. Lux, *Int. J. Refract. Met. Hard Mater.* **2002**, *20*, 51.
[14] L. Prakash, in *Proc. 13th Plansee Seminar*, Vol. *2* (Eds: H. Bildstein, R. Eck), Reutte, Austria **1993**, p. 110.
[15] J. García, *Int. J. Refract. Met. Hard Mater.* **2011**, *29*, 306.
[16] C. J. R.González Oliver, A. Caneiro, J.García, *Proc. Mater. Sci.* **2012**, *1*, 95.
[17] M. Thuvander, J. Weidow, J. Angseryd, L. K. L. Falk, F. Liu, M. Sonestedt, K. Stiller, H. O. Andén, *Ultramicroscopy* **2010**, *111*, 604.
[18] C. M. Fernandes, A. M. R. Senos, *Int. J. Refract. Met. Hard Mater.* **2011**, *29*, 405.
[19] T. W. Penrice, *J. Mater. Shaping Technol.* **1987**, *5*, 35.
[20] C. Hanyaloglu, B. Aksakal, J. D. Bolton, *Mater. Charact.* **2001**, *47*, 315.
[21] W. H. Jiang, J. Fei, X. L. Han, *J. Mater. Sci. Lett.* **2001**, *20*, 283.
[22] X. Wang, Z.Zak Fang, H. Y.Sohn, *Int. J. Refract. Met. Hard Mater.* **2008**, *26*, 232.
[23] T. Yamamoto, Y. Ikuhara, T. Sakuma, *Sci. Technol. Adv. Mater.* **2000**, *1*, 97.
[24] L. Gao, B. H. Kear, *Nanostruct. Mater.* **1997**, *9*, 205.
[25] C. Liang, F. Tian, Z. Wei, Q. Xin, C. Li, *Nanotechnology* **2003**, *14*, 955.
[26] M. J. Hudson, J. W. Peckett, P. J. F. Harris, *Ind. Eng. Chem. Res.* **2005**, *44*, 5575.
[27] J. Haber, W. Marczewski, J. Stoch, L. Ungier, *J. Solid State Chem.* **1976**, *19*, 113.
[28] C. J. R. González Oliver, P. F.James, H. Rawson, *J. Non-Cryst. Solids* **1982**, *48*, 129.
[29] C. J. R. González Oliver, M.Kume, *J. Non-Cryst. Solids* **1986**, *82*, 256.
[30] C. J. R. González Oliver, M.Schneider, K. Nawata, H. Kusano, *J. Non-Cryst. Solids* **1988**, *100*, 274.
[31] E. R. Benavidez, C. González Oliver, R. Caruso, O. de Sanctis, *Mater. Chem. Phys.* **2000**, *62*, 9.
[32] M. Omori, *Mater. Sci. Eng. A* **2000**, *287*, 183.
[33] M. C. Chou, C. F. Chu, S. T. Wu, *Mater. Chem. Phys.* **2003**, *78*, 59.
[34] E. R. Benavidez, C. J. R. González Oliver, *J. Mater. Sci.* **2005**, *40*, 3749.

DOI: 10.1002/adem.201400122